Inorganic Chemistry

Article

pubs.acs.org/IC

Structural Investigation of the Substituted Pyrochlore $AgSbO_3$ through Total Scattering Techniques

Geneva Laurita,[†] Katharine Page,[‡] A. W. Sleight,[†] and M. A. Subramanian*[,†]

[†]Department of Chemistry, Oregon State University, Corvallis, Oregon 97331, United States

[‡]Lujan Neutron Scattering Center, Los Alamos National Laboratory, LANSCE-LC, MS H805, Los Alamos, New Mexico 87545, United States

Supporting Information

ABSTRACT: Polycrystalline samples of the pyrochlore series $Ag_{1-x}M^n{}_xSbO_{3+x[(n-1)/2]}$ (M = Na, K, and Tl) have been structurally analyzed through total scattering techniques. The upper limits of x obtained were 0.05 for Na, 0.16 for K, and 0.17 for Tl. The Ag^+ cation occupies a site with inversion symmetry on a 3-fold axis. When the smaller Na^+ cation substitutes for Ag^+, it is displaced by about 0.6 Å perpendicular to the 3-fold axis to achieve some shorter Na−O bond distances. When the larger Tl^+ cation substitutes for Ag^+, it is displaced by about 1.14 Å along the 3-fold axis and achieves an environment typical of a lone pair cation. Some of the Tl^{3+} from the precursor remains unreduced, leading to a formula of $Ag_{0.772(1)}Tl^+{}_{0.13(2)}Tl^{3+}{}_{0.036(1)}SbO_{3.036(1)}$. The position of the K^+ dopant was effectively modeled assuming that K^+ occupied the same site as Ag^+. The expansion of the lattice caused by substitution of the larger K^+ and Tl^+ cations results in longer Ag−O bond lengths, which would reduce the overlap of the Ag 4d and O 2p orbitals that compose the valence band maximum. Substitution of the smaller Na^+ results in a decrease in the Ag−O bond distance, thus increasing the overlap of the Ag 4d and O 2p orbitals. This will have a direct influence on the band composition and observed properties of this material of interest.

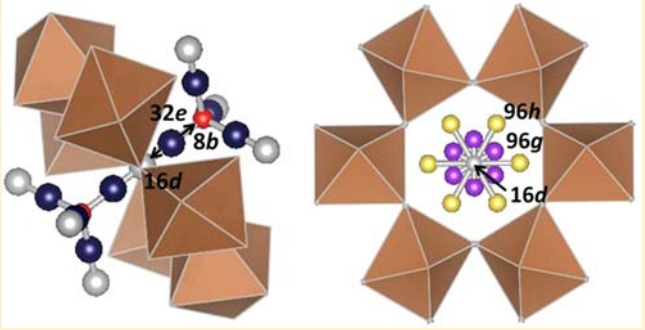

INTRODUCTION

Oxides which crystallize in the pyrochlore structure form a family of materials with fascinating properties, such as the ferroelectric $Cd_2Nb_2O_7$[1] and the superconducting $Cd_2Re_2O_7$.[2] This cubic structure is highly symmetric, belonging to the space group of $Fd\bar{3}m$. It is often represented with the formula $A_2B_2O_7$, which can be rewritten as $A_2B_2O_6O'$, as oxygen is found on two distinct crystallographic sites. The pyrochlore structure can be described as two interpenetrating three-dimensional networks: a network of corner-sharing $BO_{6/2}$ octahedra and a network of linearly coordinated A-atoms, which are linked together by a framework of O-centered tetrahedra.[3,4] The pyrochlore structure can also be described as two interpenetrating networks of corner-sharing A and B tetrahedra. The subunits of this structure allow for some of the interesting characteristics found in this family. For instance, the tetrahedral arrangement of the A and B atoms can lead to a frustrated lattice, giving rise to interesting magnetic properties.[5] The rigid octahedral framework also allows for the structure to tolerate defects in the channels where the A_2O' chains are found. In the ideal pyrochlore, the A atoms are located in the 16*d* site that is central to the $BO_{6/2}$ channel structure, and the O′ atoms are found in the 8*b* sites along this channel. In the anion-deficient pyrochlore structure, the 8*b* sites are vacant, and the resulting formula is $A_2B_2O_6$, often shortened to ABO_3. A comparison of the ideal and anion-deficient pyrochlore structure can be seen in Figure 1. While expansive, most members of the pyrochlore family crystallize in the ideal pyrochlore structure. Very few compounds can form in this family with the vacancy on the 8*b* site, and as a result, the literature on $A_2B_2O_6$ pyrochlores is relatively small. One defect pyrochlore of recent interest is $Ag_2Sb_2O_6$, often empirically referred to as $AgSbO_3$.

Discovered in 1938,[6] the defect pyrochlore $AgSbO_3$ was first structurally characterized through X-ray diffraction (XRD) by Sleight.[7] Further XRD characterization through Rietveld analysis revealed that Ag^+ sits in the center of the channel in the anion-deficient pyrochlore structure.[8] Fundamentally, this material is an Ag^+ ion conductor, and additionally displays *n*-type conductivity in bulk powders and amorphous thin-films.[9,10] Interest in the pyrochlore $AgSbO_3$ increased when photocatalytic activity was observed by powdered samples in the presence of a gaseous mixture of dry air and 2-propanol. After adsorption equilibrium was established, the sample and gaseous mixture was irradiated with visible light. Gas chromatography revealed the 2-propanol had been decomposed into acetone and molecular oxygen.[11] This visible-light response is facilitated by a narrow band gap of approximately 2.6 eV, which also led to studies of $AgSbO_3$ as a potential

Received: July 18, 2013
Published: September 10, 2013

   dx.doi.org/10.1021/ic401860j | *Inorg. Chem.* 2013, 52, 11530−11537

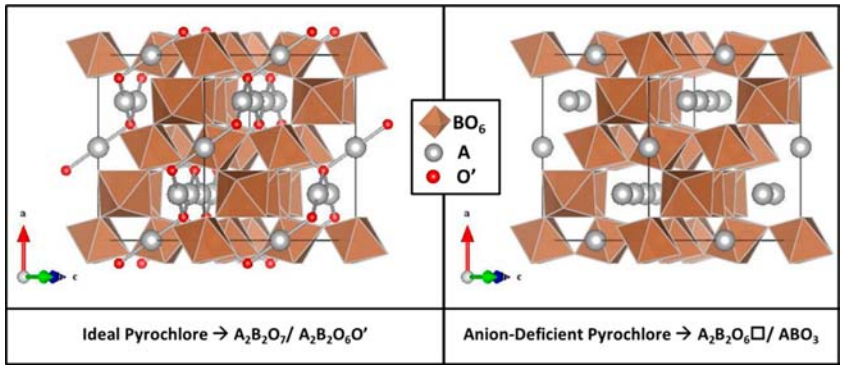

Figure 1. Crystal structure of the ideal pyrochlore $A_2B_2O_7$ (left) and its modification corresponding to the anion-deficient pyrochlore $A_2B_2O_6$ (right).

transparent conducting oxide.[10−12] The thermoelectric properties of pure $AgSbO_3$[13] and copper-doped $AgSbO_3$[14] have been systematically studied to show a maximum thermoelectric figure-of-merit, zT, of 0.06 in pure $AgSbO_3$. Copper doping increased the power factor of $AgSbO_3$, but zT was not calculated because of the absence of thermal conductivity measurements. Further studies characterized $AgSbO_3$ through scanning electron microscopy, X-ray photoelectron spectroscopy, and electron diffraction.[15] Increased photocatalytic ability has been observed in the illmenite polymorph,[16] and photocatalysis has been observed in $AgSbO_3$ prepared via ion exchange with a $NaSbO_3$ precursor.[17] Photoemission studies of $AgSbO_3$ thin-films demonstrated that the top of the valence band was primarily composed of O 2p and Ag 4d orbitals.[10] Further theoretical calculations confirmed this valence band composition, and detailed that the valence band in the anion-deficient pyrochlore was constructed of the overlap between these orbitals. This Ag 4d-O 2p orbital overlap is attributed to raising the energy of the valence band, resulting in the narrow band gap that is observed.[11,18] Theoretical studies also conclude the conduction band minimum is primarily composed of diffuse Ag 5s and Sb 5s orbitals, which also contributes to the formation of the narrow band gap that gives rise to the observed optical properties of this material.[11,12,18] In-depth studies of the pyrochlore and illmenite band structures have been performed through hybrid-density functional theory (DFT) methods to compare and contrast the two photocatalysts.[18]

To have a proper understanding of a material, an in-depth analysis of the structural characteristics must be performed. Neutron scattering can provide insight to a material that would otherwise be unattainable through XRD. In particular with oxides, neutron diffraction is essential for the structural refinement of light atom positions. As the Ag−O orbital overlap is crucial to the properties observed in this material, it is essential to employ a local probe that can sensitively identify the location of the oxygen atoms. While well-characterized, neutron studies have not been performed on $AgSbO_3$. To the best of the authors' knowledge, this is the first report of neutron diffraction studies of this compound. Furthermore, by substituting this material with metals of various electronegativities (Na, K, and Tl), the Ag−O bond length and orbital overlap will be manipulated. This manipulation will directly affect the properties in $AgSbO_3$ by changing the atom−atom interactions. Substitution will occur on the A-site of the pyrochlore structure, which sits within the large open channels of the anion-deficient pyrochlore. Upon substitution into the system, the cations on the A-site become disordered, making positional determination of the oxygen especially difficult. The ability to provide sensitivity to both the oxygen and the metals in this system makes neutron diffraction a crucial ingredient in the understanding of this promising material.

Rietveld refinement only analyzes a structure against Bragg scattering events, providing information regarding long-range crystal structures. Additional information about the structure can be obtained through total scattering, which includes not only Bragg but diffuse scattering events. After instrumental corrections are applied, the total scattering yields the reciprocal-space structure function, $S(Q)$. A sine Fourier transform of $S(Q)$ results in the pair distribution function (PDF) of the sample, $G(r)$. The PDF is a distribution of all atom−atom correlations occurring at real-space distances, and provides experimental access to the local structure of a sample.[19]

The use of the neutron PDF is essential for the determination of the local structure in $Ag_{1-x}M^n_xSbO_{3+x[(n-1)/2]}$ (M = Na, K, and Tl). Employing neutron total scattering will help determine the oxygen environment on the average and local scale, providing a better understanding of the disorder in the structure. This analysis will provide a detailed account of the effect of substitution upon the Ag−O bond length, which will give insight to how the Ag 4d-O 2p orbital overlap is changing upon doping. A change in orbital overlap could have a major effect on the properties observed in $AgSbO_3$. This work aims to use total scattering techniques to determine the local and average structure of the pyrochlore $AgSbO_3$ and to determine the effects of substitution on the anion-deficient structure.

■ EXPERIMENTAL SECTION

Samples were made through standard solid state synthesis techniques by mixing stoichiometric amounts of high purity Ag_2O, Sb_2O_3, and either K_2CO_3, Na_2CO_3, or Tl_2O_3. After being thoroughly ground, the mixtures were pelletized and annealed at 750 °C (Na, K) or 500 °C (Tl) for 12 h. Powders were first characterized through XRD to verify phase purity with a Rigaku Miniflex II diffractometer using Cu Kα radiation and a graphite monochromator on the diffracted beam. Powder samples were loaded onto a "zero background" oriented silicon single crystal sample holder (MTI corp.) to maximize the detection of minor impurity phases. Data was collected from 10 to 120° 2θ with a step size of 0.02° 2θ and a dwell time of 2.0 s. Time-of-flight (TOF) neutron scattering data was collected on powdered samples on the NPDF instrument at Los Alamos National Laboratory.[20] Approximately 3−4 g of sample were placed into vanadium cans, and measurements were obtained at 298 K for approximately 4 h. Rietveld refinements were conducted using the

dx.doi.org/10.1021/ic401860j | Inorg. Chem. 2013, 52, 11530−11537

GSAS software with the interface EXPGUI.[21,22] Because of the relatively high absorption cross-section of Ag, an absorption correction was applied to all data. Data reduction to obtain the PDF $G(r)$ function was performed using the PDFgetN program,[23] with Q_{max} = 35 Å^{-1}, which was selected to balance between resolution and termination ripples in the reduced data. Least-squares refinement of reduced PDF functions were performed with PDFGUI.[24] While local refinements were performed for various ranges of real space data (r = 1.7−5 Å, r = 1.7−10 Å, and r = 1.7−20 Å), the dependency of the parameters on the range was determined to be negligible. Therefore, the reported PDF refinements have been completed with a 1.7 to 10 Å range.

STRUCTURAL ANALYSIS

Initial structural lattice parameters were refined through the Le Bail method.[25] All peaks were indexed as cubic with the space group $Fd\bar{3}m$ for nominal values of x = 0−0.2 for the series $Ag_{1-x}M^{n}_{x}SbO_{3+x[(n-1)/2]}$ (M = Na and Tl) and x = 0.33 for the series $Ag_{1-x}K_xSbO_3$, indicating a solubility limit in the pyrochlore structure for Tl, Na, and K. Lattice parameters increased upon Tl and K substitution, as is expected when the larger K^+ (r_{ionic} = 1.38 Å) and Tl^+ (r_{ionic} = 1.50 Å) ions replace Ag^+ (r_{ionic} = 1.15 Å).[26] The lattice parameter was unchanging for Na substitution, which will be discussed further in the detailed analysis of the Na-substituted samples. An evolution of the lattice parameter upon substitution can be seen in Figure 2 for the neutron Rietveld refinements. Neutron lattice parameters are in reasonable agreement with XRD lattice parameters.

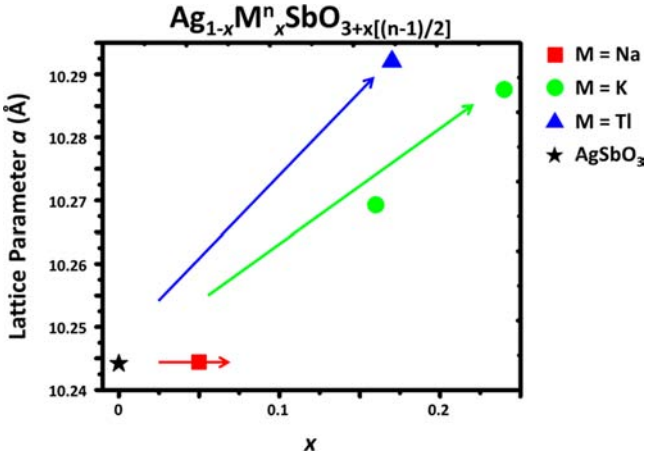

Figure 2. Lattice parameter evolution determined from neutron diffraction Rietveld analysis as cations Na, K, and Tl are doped into $AgSbO_3$. Error bars are contained within the points.

A summary of selected crystallographic parameters from the neutron Rietveld for all samples can be found in Table 1. Average and local structure refined atomic positional and displacement parameters for all samples are summarized in Table 2. Detailed results of the local PDF refinements can be found in Supporting Information, Table S1. Local refinements were performed with occupancies fixed to those obtained through neutron Rietveld refinements of the average structure.

Average structure refinements of the parent compound $AgSbO_3$ assumed full occupancy for antimony and oxygen and all ideal positions were occupied: Ag in 16*d*, Sb in 16*c*, and O in 48*f*. Rietveld analysis indicates that the ideal positions provide a good fit for the experimental data. Local refinements of $AgSbO_3$ agree with the average model, indicating disorder of the Ag^+ on the A-site within the channel structure. The displacement is evidenced through average and local fitting of the Ag^+ anisotropic atomic displacement parameters. The primary displacement along the 3-fold axis is as expected, as this is the direction of the missing O′ atom with respect to the $A_2B_2O_6O'$ formula for the pyrochlore structure. The Rietveld and local fit, along with a pictorial representation of the displacement of Ag^+ can be found in Figure 3.

The atom−atom correlations that form the PDF of $AgSbO_3$ can easily be identified by calculating the individual partials of each type of atom−atom pair in the compound, shown in Figure 4. By referencing the partials, each peak in the PDF can be assigned to a bond length in the structure. The first peak in the PDF is formed entirely by Sb−O correlations, and this can be assigned to the basic octahedral SbO_6 unit that forms the corner-sharing octahedral network. The first major Ag−O partial peak at approximately 2.55 Å can similarly be assigned to the bonds between silver and oxygen that form the channel structure. This is also the bond that contributes to the valence band maximum, and is the primary bond length that will be probed through doping.

Initial Rietveld refinements of the substituted samples were performed on samples assuming all cations were substituted directly for Ag^+ on the 16*d* site. Antimony and oxygen content was fixed at full occupancy, as was done with $AgSbO_3$. As there is a large space within the BO_6 channels, the A atom could potentially displace off of this ideal site. A displacement perpendicular to the 3-fold rotation axis of the channel results in the A atom occupying the variable 96*h* or 96*g* sites, and a displacement parallel to the rotation axis results in an occupancy of the variable 32*e* site. These various displacements are shown in Figure 5, and will be explored as options for the location of the A cation upon substitution in the average and local structure data.

Table 1. Crystallographic Data from the Rietveld Refinement of Neutron Diffraction Data for the Series $Ag_{1-x}M^{n}_{x}SbO_{3+x[(n-1)/2]}$ (M = Na, K, and Tl)

chemical formula	$AgSbO_3$	$Ag_{0.96(1)}Na_{0.05(1)}SbO_3$	$Ag_{0.83(3)}K_{0.16(3)}SbO_3$	$Ag_{0.76(4)}K_{0.24(4)}SbO_3$	$Ag_{0.772(1)}Tl^{+}_{0.13(2)}Tl^{+3}_{0.036(1)}SbO_{3.036(1)}$
a (Å)	10.2442(3)	10.2444(3)	10.2693(2)	10.2875(3)	10.292(1)
volume (Å^3)	1075.0(1)	1075.12(2)	1082.9(2)	1088.7(1)	1090.2(2)
Z	16	16	16	16	16
formula weight	277.62	274.87	266.55	261.78	298.54
space group	$Fd\bar{3}m$	$Fd\bar{3}m$	$Fd\bar{3}m$	$Fd\bar{3}m$	$Fd\bar{3}m$
temperature (°C)	25	25	25	25	25
density$_{calc}$ (g/cm^3)	6.86	6.79	6.54	6.39	7.28
R (%)	2.16	2.02	2.55	2.39	2.02
R_{wp} (%)	3.36	3.26	3.77	3.56	3.17

dx.doi.org/10.1021/ic401860j | Inorg. Chem. 2013, 52, 11530−11537

Table 2. Refined Atomic Positional and Displacement Parameters from Average (Rietveld) and Local (PDF) Structure Refinements for the Series $Ag_{1-x}M^{n}_{x}SbO_{3+x[(n-1)/2]}$ (M = Na, K, and Tl) from Neutron Data[a]

	$AgSbO_3$		$Ag_{0.96(1)}Na_{0.05(1)}SbO_3$		$Ag_{0.83(3)}K_{0.16(3)}SbO_3$		$Ag_{0.76(4)}K_{0.24(4)}SbO_3$		$Ag_{0.772(1)}Tl^{+}_{0.13(2)}Tl^{+3}_{0.036(1)}SbO_{3.036(1)}$	
parameter	NPDF	Rietveld	NPDF	Rietveld	NPDF	Rietveld	NPDF	Rietveld	NPDF	Rietveld
O (48*f*) *x*	0.324(1)	0.323(3)	0.324(1)	0.324(1)	0.323(1)	0.323(3)	0.323(1)	0.322(2)	0.322(1)	0.3223(3)
Na^{+} (96*h*) *y*			0.43(2)	0.458(1)						
Tl^{+} (32*e*) *x*									0.432(3)	0.436(2)
Ag^{+} $U_{11}(Å^2)^b$	0.027(2)	0.027(3)	0.029(2)	0.027(1)	0.060(4)	0.052(2)	0.08(1)	0.076(1)	0.033(2)	0.031(2)
$U_{12}(Å^2)^b$	0.016(2)	0.015(1)	0.016(2)	0.015(1)	0.047(4)	0.040(3)	0.07(1)	0.0064(3)	0.01(3)	0.010(2)
M $U_{11}(Å^2)^b$			0.03(1)	0.017(3)	0.060(4)	0.052(2)	0.08(1)	0.076(1)	0.022(1)	0.01(1)
$U_{12}(Å^2)^b$			0	0	0.047(4)	0.040(3)	0.07(1)	0.0064(3)	0	0
Sb U_{iso} ($Å^2$)	0.0028(2)	0.0048(2)	0.0027(2)	0.004(2)	0.0031(2)	0.0043(1)	0.0035(2)	0.0047(1)	0.0035(3)	0.0044(1)
O (48*f*) $U_{11}(Å^2)$	0.0070(4)	0.009(1)	0.007(12)	0.009(1)	0.0088(1)	0.0104(1)	0.008(1)	0.0107(2)	0.008(1)	0.010(1)
$U_{22}(Å^2)$	0.0091(3)	0.010(1)	0.009(2)	0.0097(4)	0.0097(3)	0.0098(1)	0.0095(3)	0.0096(2)	0.0102(4)	0.010(1)
$U_{33}(Å^2)$	0.0091(3)	0.010(1)	0.009(2)	0.0097(4)	0.0097(3)	0.0098(1)	0.0095(3)	0.0096(2)	0.0102(4)	0.010(1)
$U_{12}(Å^2)$	0	0	0	0	0	0	0	0	0	0
$U_{13}(Å^2)$	0	0	0	0	0	0	0	0	0	0
$U_{23}(Å^2)$	0.0068(3)	0.005(1)	0.006(2)	0.005(4)	0.0069(1)	0.0060(1)	0.006(1)	0.0062(1)	0.007(1)	0.007(1)
O (8*b*) U_{iso} ($Å^2$)									0.032(3)	0.04(3)

[a]PDF refinements were completed on the *r*-range 1.7−10 Å. [b]$U_{11} = U_{22} = U_{33}$, $U_{12} = U_{13} = U_{23}$.

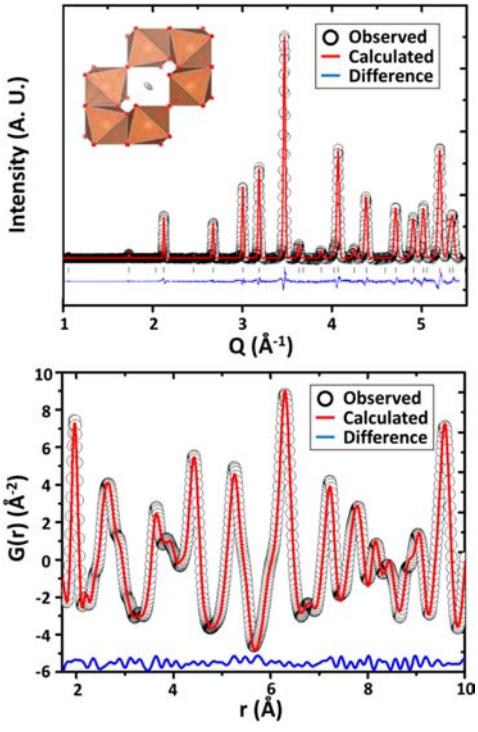

Figure 3. Average Rietveld (top) and local PDF (bottom) structure fits to the neutron data for the parent compound $AgSbO_3$. Refinements indicate the atomic displacement of the Ag^{+} cation is parallel to the 3-fold rotation axis of the structure (top, inset).

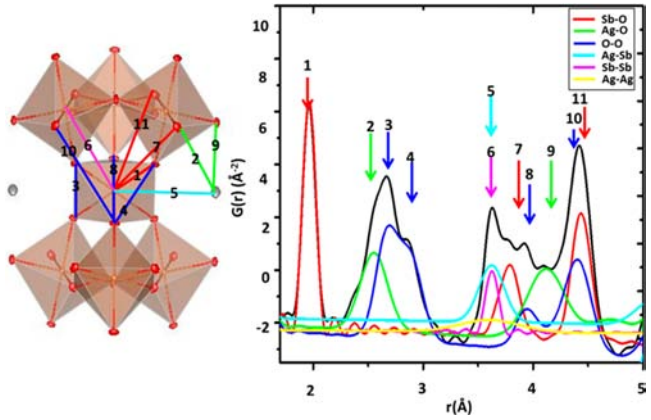

Figure 4. Partial atom−atom contributions to the PDF function in the range of 1.7−5 Å. Peaks within the PDF can be assigned to various atom−atom correlations in the anion-deficient pyrochlore $AgSbO_3$. The black curve related the total PDF, while colored curves correspond to specific partial contributions.

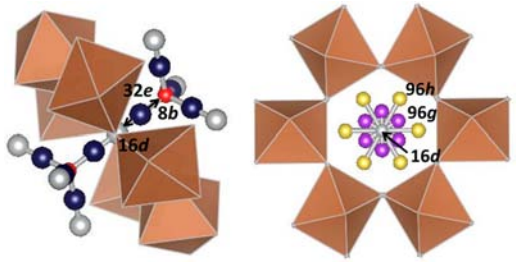

Figure 5. Schematic representation of the available sites for the A cation within the $BO_{6/2}$ channel structure. The ideal position for the A cation is 16*d*. Red atoms at 8*b* indicate regular pyrochlore locations for the O′ positions. Arrows along the 3-fold rotation axis indicate the displacement direction of the 32*e* site, shown in purple.

The observation of unchanged lattice parameters upon Na^{+} substitution suggests that as Na^{+} is introduced into the structure, the $SbO_{6/2}$ octahedral network remains nearly unchanged. Thus, we assumed that the displacement parameters of Ag^{+} should be unchanged as well upon substitution. Therefore, our model for refinement fixed the displacement parameters for Ag^{+} at the values obtained for $AgSbO_3$. The atomic displacement factor for Na was refined independently and found to be so large that we evaluated a model in which Na was statically displaced from the Ag site. The site for Ag is 16*d* ($^1/_2$, $^1/_2$, $^1/_2$), and the 96*h* site ($^1/_2$, *y*, −*y*) allows Na to displace off this site in a direction perpendicular to the 3-fold axis providing some shorter Na−O bonds. Rietveld refinements indicate that when modeled in

dx.doi.org/10.1021/ic401860j | *Inorg. Chem.* 2013, 52, 11530−11537

96*h* there is a Na displacement of about 0.6 Å off the 3-fold axis. However, the obtained R_{wp} value of this model was very similar to that of the 16*d* model with a larger isotropic dynamic displacement, and it was difficult to determine the most accurate description of the structure through Rietveld refinements. Local modeling of Na in the 96*h* site in the PDF data revealed a reduction in both the atomic displacement of Na and R_{wp} in comparison to the 16*d* model, indicating that Na^+ does indeed occupy this site. Bond valence sum (BVS) calculations also support this, and a comparison between the refined values and the BVS calculations for the two models can been seen in Table 3. Rietveld fits of the Na sample can be seen in Supporting Information, Figures S1–S2.

Table 3. Comparison of the Refined Atomic Positional and Displacement Parameters from Average (Rietveld) and Local (PDF) Structure Refinements for the Series $Ag_{1-x}M^n_xSbO_{3+x[(n-1)/2]}$ (M = Na, K, and Tl) from Neutron Data[a]

	$Ag_{0.96(1)}Na_{0.05(1)}SbO_3$			
	PDF		Rietveld	
parameter	Na^+ in 16*d*	Na^+ in 96*h*	Na^+ in 16*d*	Na^+ in 96*h*
BVS, Na^+	0.78	1.17	0.80	1.26
R_{wp} (%)	7.45	7.11	3.26	3.26
Na^+, *y*	0.5	0.461(3)	0.5	0.458(1)
Ag U_{11}(Å^2)[b]	0.028(1)	0.029(2)	0.027(1)	0.027(1)
U_{12}(Å^2)[b]	0.0162(2)	0.016(2)	0.015(1)	0.015(1)
Na^+ U_{iso}(Å^2)	0.22(3)	0.03(1)	0.10(1)	0.017(3)

[a]PDF refinements were completed on the *r*-range 1.7–10 Å. [b]$U_{11} = U_{22} = U_{33}$, $U_{12} = U_{13} = U_{23}$.

Because of size and electronic configuration, refinements of the K^+ substituted samples were performed with the assumption that K^+ would behave similarly to Ag^+, and the atomic displacement parameters for the A-site cations were constrained to be equivalent during average structure modeling. The large cage at the A-site results in larger displacement factors, which remain highly anisotropic. This high degree of anisotropic movement along the 3-fold rotation axis is also observed in the local PDF refinements. Rietveld and local PDF fits are contained in the Supporting Information, Figures S3–S6.

Initial refinements of the sample substituted with Tl indicated that Tl was strongly displaced from the Ag site. In this case (contrary to Na case), it was found that Tl remains on the 3-fold axis but is in the 32*e* site very strongly displaced (1.14 Å) from the 16*d* (Figure 6). The Tl–O distances for Tl^+ on the 16*d* would be much too small for Tl^+, giving a Tl bond valence sum of 1.84. After the displacement of 1.14 Å the bond valence sum for this Tl^+ becomes 1.09. Since there is the possibility that some of the precursor Tl^{3+} remains unreduced, the occupancy of an O atom in the 8*b* site was refined. The obtained value of 0.036(1) indicates a formula of $Ag_{0.772(1)}Tl^+_{0.13(2)}Tl^{3+}_{0.036(1)}SbO_{3.036(1)}$. The size of Tl^{3+} is close enough to that of Ag^+ that it was assumed that the Tl^{3+} would be on the Ag^+ site, and the final formula was obtained with this assumption. The environment of Tl^+ (Figure 7) with all strong bonds on one side is that expected for a lone pair cation. The lone pairs of Tl^+ would be pointed in the direction of the 8*b* site, which should be empty because the small amount of O in this site would be attracted to the vicinity of Tl^{3+}. A complete summary of refined parameters and fits for all models can be found in the Supporting Information, Figures S7–S11 and Table S2.

DISCUSSION

As previously discussed, a very rigid and unchanging $SbO_{6/2}$ network is present. This was initially concluded from an unchanging lattice parameter upon Na^+ substitution, but can be further evidenced by directly comparing the first 3 Å of the local PDF data of $AgSbO_3$ with the highest-substituted sample for each element, shown in Figure 8. The primary Sb–O correlation peaks overlay almost completely, whereas the peak for the Ag–O correlation changes quite drastically. Through an analysis of the local data, it can be seen that the Sb–O correlation and consequently the $SbO_{6/2}$ network remains relatively unchanged throughout the entire series $Ag_{1-x}M^n_xSbO_{3+x[(n-1)/2]}$ (M = Na, K, and Tl).

Selected bond distances and bond angles from the Rietveld and PDF fits are summarized in Table 4, and Figure 9 relates bond length and bond angle results from the Rietveld analysis of the samples series. In Figure 9a we see that Ag–O bond length increases as expected as the larger K^+ and Tl^+ substitute for Ag^+. We also see that substituting Na^+ for Ag^+ causes a decrease in the average Ag–O distance. This is not surprising except for the fact that there is no noticeable decrease in the lattice parameter as Na^+ substitutes for Ag^+. This decrease of the Ag–O distance with no decrease in the lattice parameter can only occur if there is a compensating increase in the Sb–O distance. Such an increase does appear to occur, albeit very small. A plot of the Sb–O distance (Figure 9b) vs *x* indicates a small but steady increase in the Sb–O distance as *x* increases

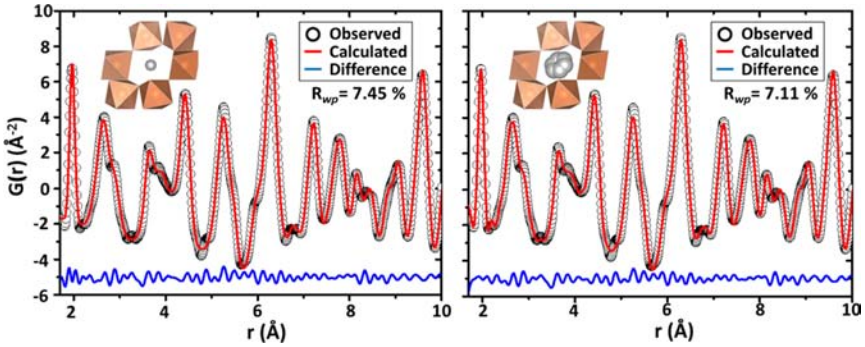

Figure 6. Local refinement fit results to neutron data for the various sodium models. Refinement fits for the sample $Ag_{0.96(1)}Na_{0.05(1)}SbO_3$ where sodium sits in the 16*d* site (left) and 96*h* site (right).

dx.doi.org/10.1021/ic401860j | *Inorg. Chem.* 2013, 52, 11530–11537

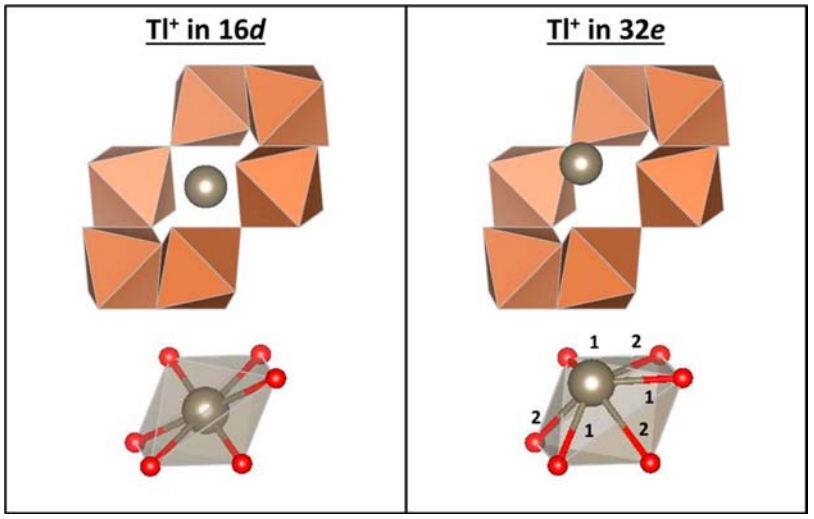

Figure 7. Coordination environment for Tl^+ in 16*d* (left) vs 32*e* (right). When located in 16*d*, Tl^+ has six equivalent Tl−O bonds (2.579 Å), whereas when located in the 32*e* site, short (bonds #1, 2.636 Å) and long (bonds #2, 2.98 Å) Tl−O bonds are observed. Movement into 32*e* results in a displacement of 1.14 Å off of the 16*d* site.

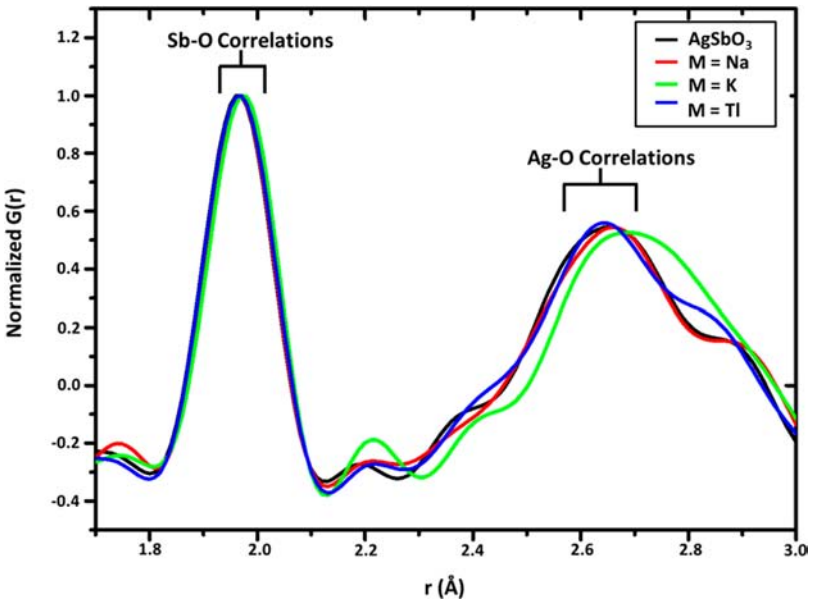

Figure 8. Overlay of the PDF data in the range of 1.7−3 Å. Peaks within the PDF can be assigned to various atom−atom correlations in the defect pyrochlore $AgSbO_3$. The black curve corresponds to the total PDF, while colored curves correspond to various samples in the series $Ag_{1-x}M^n{}_xSbO_{3+x[(n-1)/2]}$ (M = Na, K, and Tl). For M = K, the atom−atom correlation curve for $Ag_{0.76(4)}K_{0.24(4)}SbO_3$ is shown.

Table 4. Selected Bond Lengths and Angles from Average (Rietveld) and Local (PDF) Structure Refinements for the Series $Ag_{1-x}M^n{}_xSbO_{3+x[(n-1)/2]}$ (M = Na, K, and Tl) from Neutron Data[a]

	$AgSbO_3$		$Ag_{0.96(1)}Na_{0.05(1)}SbO_3$		$Ag_{0.83(3)}K_{0.16(3)}SbO_3$		$Ag_{0.76(4)}K_{0.24(4)}SbO_3$		$Ag_{0.772(1)}Tl^+_{0.13(2)}T\text{-}I^{+3}_{0.036(1)}SbO_{3.036(1)}$	
parameter	NPDF	Rietveld	NPDF	Rietveld	NPDF	Rietveld	NPDF	Rietveld	NPDF	Rietveld
Ag−O (Å)	2.558(1)	2.555(1)	2.556(1)	2.554(1)	2.570(1)	2.566(1)	2.576(2)	2.574(1)	2.581(2)	2.577(1)
M−O (Å)			3.04(3)	3.08(2)	2.570(1)	2.566(1)	2.576(2)	2.574(1)	2.660(4)	2.636(2)
			2.61(1)	2.62(3)					3.02(1)	2.98(2)
			2.10(3)	2.06(1)						
Sb−O (Å)	1.966(1)	1.963(1)	1.966(1)	1.963(1)	1.968(1)	1.965(1)	1.970(1)	1.966(1)	1.968(1)	1.966(1)
Ag−O−Ag (deg)	62.8(1)	62.8(1)	62.9(1)	62.8(1)	62.8(1)	62.8(2)	62.7(2)	62.7(1)	62.7(1)	62.7(3)
Sb−O−Sb (deg)	134.54(2)	134.57(1)	134.43(2)	134.48(1)	134.90(1)	134.86(2)	135.17(1)	135.41(1)	135.41(2)	135.33(1)

[a]PDF refinements were completed on the *r*-range 1.7−10 Å.

dx.doi.org/10.1021/ic401860j | *Inorg. Chem.* 2013, 52, 11530−11537

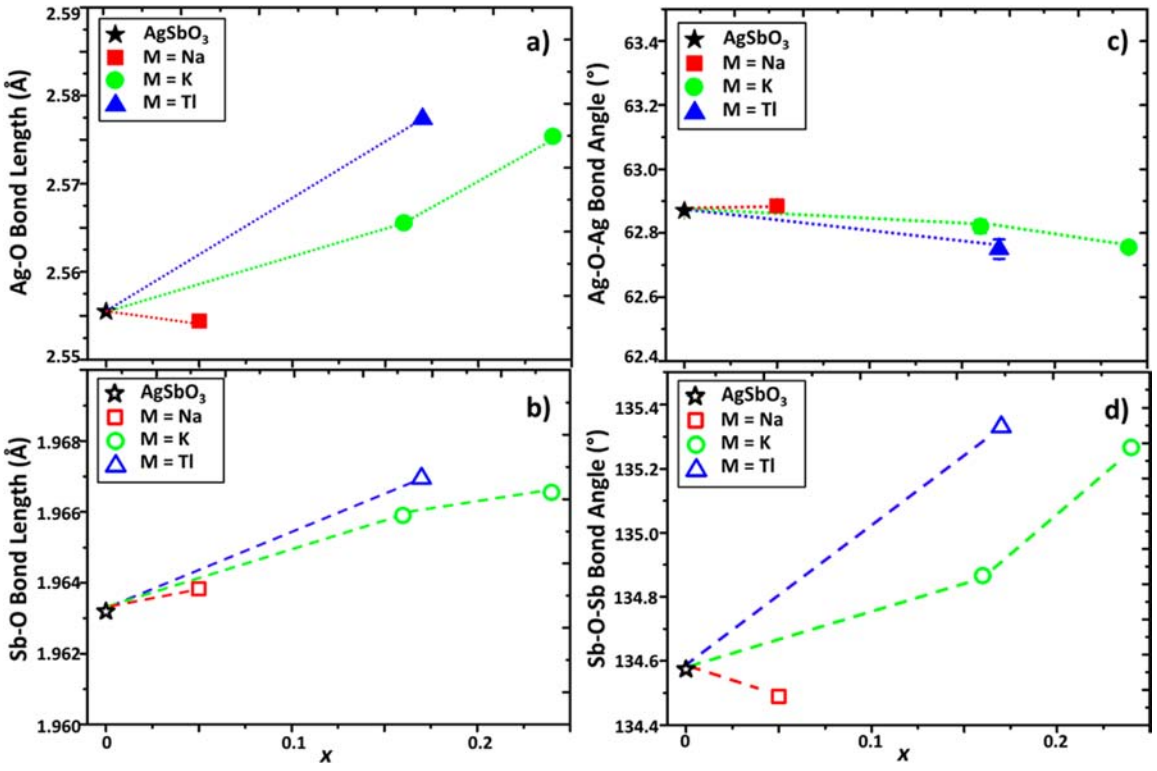

Figure 9. Ag−O bond length (top, left), Sb−O bond length (bottom, left), Ag−O−Ag bond angle (top, right), and Sb−O−Sb bond angle (bottom, right) evolution in the series $Ag_{1-x}M^{n}_{x}SbO_{3+x[(n-1)/2]}$ (M = Na, K, and Tl) as determined by Rietveld refinement of the neutron data. Error bars are contained within the point for plots a, b, and d.

for all samples. As the Ag−O bond length increases in the material, the amount of overlap between the silver and oxygen orbitals will decrease and conversely, as the bond length decreases, the overlap will increase. While the Sb−O bond length apparently increases as the system is doped, the change is not as great in magnitude as the change upon doping of the Ag−O bond. Therefore, doping has a larger effect on the environment of the channel structure, leaving the SbO_6 octahedral network relatively unchanged. As the valence band maxima is composed primarily of the orbital overlap between Ag 4s and O 2p orbitals, a manipulation of the Ag−O bond length will directly change the character of the upper valence band. With overlap between Ag 4s and O 2p, the energy of the valence band is increased, giving rise to a narrow band gap. Therefore, a decrease in the orbital overlap should result in a lowering of the energy, and an increase in the observed band gap, or vice versa. If the magnitude of the band gap is changed, this will change the wavelength of light that promotes the properties observed in $AgSbO_3$. The amount of overlap will be affected not only by the M−O bond distance, but also the M−O−M bond angles. Figure 9c and 9d show the change in Ag−O−Ag and Sb−O−Sb bond angle upon doping, respectively. The Ag−O−Ag angle remains relatively unchanged, indicating the Ag−O bond distance will have the largest effect on the orbital overlap. The Sb−O−Sb angle does show a change as various metals are doped into the system, but this should not have a major influence on the Ag−O orbital overlap. Therefore, by these observations, it is predicted that substitution of K^+ and Tl^+ will result in a weaker orbital overlap and larger band gap, while substitution by Na^+ will lead to a stronger overlap and smaller band gap. Substitutions into the A-site by other cations may result in a decrease in the ionic conductivity of Ag^+ in the system, particularly in the samples with nonideal positions occupied. To get a full understanding of the material relationships, detailed optical and electrical analysis is in progress. However, by taking an in-depth look at the structural changes upon substitution, the effect on bond distances and angles can be analyzed, and a prediction of the effects on sample properties can be made. These insights will contribute to accelerated materials' design via optimization of such structure−property effects.

■ ASSOCIATED CONTENT

Supporting Information

Neutron crystallographic data in CIF format for $Ag_{1-x}M^{n}_{x}SbO_{3+x[(n-1)/2]}$ (M = Na, K, and Tl) phases. Data summary from PDF data refinements for $Ag_{1-x}M^{n}_{x}SbO_{3+x[(n-1)/2]}$ (M = Na, K, and Tl). Data summary from the various models for the average Rietveld and local PDF refinements for the sample with nominal composition $Ag_{0.8}Tl_{0.2}SbO_3$. Additional figures for the average Rietveld and local PDF refinements. This material is available free of charge via the Internet at http://pubs.acs.org.

■ AUTHOR INFORMATION

Corresponding Author

*E-mail: mas.subramanian@oregonstate.edu.

Notes

The authors declare no competing financial interest.

■ ACKNOWLEDGMENTS

This work was supported by NSF Grant CHE-1102637. We thank Joan Siewenie at Los Alamos National Laboratory for her assistance with the neutron data collection and reduction, and

Dr. Jun Li for her helpful discussions in regards to Rietveld analysis. This work benefitted from the use of NPDF at the Lujan Center at Los Alamos Neutron Science Center, funded by DoE BES. Los Alamos National Laboratory is operated by Los Alamos National Security LLC under DoE Contract DEAC52-06NA25396. The upgrade of NPDF was funded by the National Science Foundation through Grant DMR 00-76488.

REFERENCES

(1) Jona, F.; Shirane, G.; Pepinsky, R. *Phys. Rev.* **1955**, *98*, 903−909.
(2) Jin, R.; He, J.; McCall, S.; Alexander, C.; Drymiotis, F.; Mandrus, D. *Phys. Rev. B: Condens. Matter* **2001**, *64*, 180503.
(3) Sleight, A. W. *Inorg. Chem.* **1968**, *7*, 1704−1708.
(4) Subramanian, M. A.; Aravamudan, G.; Subba Rao, G. V. *Prog. Solid State Chem.* **1983**, *15*, 55−143.
(5) Gardner, J. S.; Gingras, M. J. P.; Greedan, J. E. *Rev. Mod. Phys.* **2010**, *82*, 53−107.
(6) Schrewelius, N. *Z. Anorg. Chem.* **1938**, *238*, 241.
(7) Sleight, A. W. *Mater. Res. Bull.* **1969**, *4*, 377−380.
(8) Zarbin, A. J. G.; Alves, O. L.; Amarilla, J. M.; Rojas, R. M.; Rojo, J. M. *Chem. Mater.* **1999**, *11*, 1652−1658.
(9) Matsumoto, Y.; Funaki, K.; Hombo, J.; Ogawa, Y. *J. Solid State Chem.* **1992**, *99*, 336−342.
(10) Yasukawa, M.; Hosono, H.; Ueda, N.; Kawazoe, H. *Solid State Commun.* **1995**, *95*, 399−403.
(11) Kako, T.; Kikugawa, N.; Ye, J. *Catal. Today* **2008**, *131*, 197−202.
(12) Mizoguchi, H.; Eng, H. W.; Woodward, P. M. *Inorg. Chem.* **2004**, *43*, 1667−1680.
(13) Sang, H.-Y.; Li, J.-F. *J. Alloys Compd.* **2010**, *493*, 678−682.
(14) Nishiyama, S.; Ichikawa, A.; Hattori, T. *J. Ceram. Soc. Jpn.* **2004**, *112*, 298−300.
(15) Yi, Z. G.; Liu, Y.; Withers, R. L. *J. Appl. Phys.* **2010**, *108*, 024911.
(16) Singh, J.; Uma, S. *J. Phys. Chem. C* **2009**, *113*, 12483−12488.
(17) Liu, W.; Liu, X.; Fu, Y.; You, Q.; Huang, R.; Liu, P.; Li, Z. *Appl. Catal., B* **2012**, *123−124*, 78−83.
(18) Allen, J. P.; Nilsson, M. K.; Scanlon, D. O.; Watson, G. W. *Phys. Rev. B: Condens. Matter* **2011**, *83*, 035207.
(19) Egami, T.; Billinge, S. J. L. *Underneath the Bragg Peaks: Structural Analysis of Complex Materials*; Pergamon: New York, 2003; Vol. 7.
(20) Proffen, T.; Egami, T.; Billinge, S. J. L.; Cheetham, A. K.; Louca, D.; Parise, J. B. *Appl. Phys. A: Mater. Sci. Process.* **2002**, *74*, s163−s165.
(21) Larson, A. C.; Von Dreele, R. B. *General Structure Analysis System (GSAS)*; Los Alamos National Laboratory Report LAUR 89-748; Los Alamos National Laboratory: Los Alamos, NM, 1994.
(22) Toby, B. H. *J. Appl. Crystallogr.* **2001**, *34*, 210−213.
(23) Peterson, P. F.; Gutmann, M.; Proffen, T.; Billinge, S. J. L. *J. Appl. Crystallogr.* **2000**, *33*, 1192−1192.
(24) Farrow, C. L.; Juhas, P.; Liu, J. W.; Bryndin, D.; Božin, E. S.; Bloch, J.; Proffen, T.; Billinge, S. J. L. *J. Phys.: Condens. Matter* **2007**, *19*, 335219.
(25) Le Bail, A. *Powder Diffr.* **2005**, *20*, 316−326.
(26) Shannon, R. D. *Acta Crystallogr., Sect. A: Found. Crystallogr.* **1976**, *32*, 751−767.